

• Supplementary File •

Strategies for Mitigating Detrimental Effects in Cyber-Physical Multiplex Networks

Yudong GONG¹, Shenghai YANG¹, Sanyang LIU^{1*}, Pei WANG¹ & Yiguang BAI^{1*}

¹*School of Mathematics and Statistics, Xidian University, Xi'an, 710126, China*

Appendix A Preliminaries and Notations

Appendix A.1 Related Works

Lack of communication is believed to be the main causes of failure for immunization campaigns [1], this inspires works to conduct the investigation on a kind of Epidemic-Awareness Coupling Mechanism (EACM). A seminal contribution in this domain was made by Funk et al. [2], who introduced an epidemiological model, and unveiled the pivotal role of awareness diffusion in mitigating the scale of epidemic outbreaks. Granell et al. [3] found the emergence of a meta-critical point wherein the onset of epidemics becomes intricately regulated by the diffusion of information, shedding valuable light on this complex interplay. In a subsequent development, they [4] had further extended their model to investigate the impact of self-awareness and mass media on dynamics. Remarkably, this exploration revealed that the meta-critical point disappears due to the mass media. Recently, Liu et al. [5] explored individual variances in information acceptance and protective measures against epidemics. Yin et al. [6] developed a three-layered network model to examine the coevolution of negative vaccine-related information, vaccination behavior, and epidemic spread, determining that the vaccination rate and the topology of epidemic spread layer are pivotal in defining the epidemic threshold. Yang et al. [7] extended the EACM to encompass time-varying multiplex networks, delving into the complex dynamics driven by asymmetric interactions over time. Guo et al. [8] analyzed a partial mapping relationship between two layers, in which only pairwise nodes have correspondence, and the individual with knowledge of prevention information will take effective measures to avoid being infected. Furthermore, as the future state of an individual at any given time depends only on its current state and is independent of past states, the Microscopic Markov Chain Approach (MMCA) is extensively used to model epidemic diffusion dynamics within EACM [9,10].

The Epidemic-Rumor Spreading Mechanism (ERSM) concentrates on mitigating the detrimental effects of epidemics and rumors, concurrently. The application of evolutionary multi-objective optimization algorithms has gained significant traction across various research domains. These algorithms are generally categorized into three groups: i) Pareto-based, such as NSGA-II [11], SPEA2 [12]; ii) Decomposition-based, such as MOEA/D [13], and iii) Indicator-based, such as Hypervolume metric [14]. Their efficacy in identifying critical nodes or maximizing influence is well-documented across various studies [15–20].

Appendix A.2 Cyber-Physical Multiplex Networks

Multiplex networks offer a sophisticated framework where nodes maintain invariant identities across numerous interconnected layers, while displaying distinct connections and dynamics within each layer. By splitting the overall systems into component networks, new phenomena can be uncovered and predicted [21]. The spread of epidemics typically occurs through physical contact networks, mirroring offline campaigns, while the propagation of information is prevalent within cyber-communication networks, akin to online campaigns. Historically, various researches had largely treated these processes independently, yet real-world instances frequently demonstrate interactions or couplings between them [3].

The present paper delves into intricacies of a multiplex network denoted as $G := \langle C, P \rangle$, which is composed of two single layer networks. The upper layer denoted as $C := \langle V, E_C \rangle$ is the cyber-communication network where information spreads. Conversely, the lower layer denoted as $P := \langle V, E_P \rangle$, represents the physical contact network where disease spreads. Notably, both layers share an identical vertex set $V = \{v_1, v_2, \dots, v_n\}$ while with distinct intra-link topologies: $E_C = \{e_1^c, e_2^c, \dots, e_m^c\}$ and $E_P = \{e_1^p, e_2^p, \dots, e_w^p\}$. Furthermore, the adjacency matrix of C is represented as $\{a_{ij}\}_{n \times n}$, where $\{a_{ij}\} = 1$ signifies the presence of a link from node v_i to v_j within in layer C , while $\{a_{ij}\} = 0$ denotes the absence of such a link. Analogously, b_{ij} adheres to a comparable definition within the context of layer P .

Then, we explore the dynamics of epidemic transmission within a community-structured layer P , where community characteristics embody significant geopolitical elements integral to social networks, elucidates the process of initial localized epidemic spread within communities, succeeded by wider network dissemination. In parallel, layer C categorizes information propagation campaigns into two types: i) positive communications, such as awareness campaigns, which amplify individuals' perception of epidemic risk and advocate for protective measures; ii) negative communications, such as rumors, which are particularly pervasive in the context of an epidemic outbreak. This integration of epidemic processes with both positive and negative informational content gives rise to the emergence of two novel mechanisms: Epidemic-Awareness Coupling Mechanism (EACM) and Epidemic-Rumor Spreading Mechanism (ERSM).

* Corresponding author (email: sylu@xidian.edu.cn, ygbai@foxmail.com)

Appendix B Methodologies in EACM

Appendix B.1 Propagation Dynamics

We implement the Susceptible-Infectious-Susceptible (SIS) model for the physical layer (P) and the Unaware-Aware-Unaware (UAU) model for the cyber layer (C). In layer P , the parameter β denotes the probability that a susceptible individual becomes infected, while μ denotes the spontaneous recovery probability for an infected node. In layer C , the analogous roles of β and μ are represented by φ and δ , respectively. Therefore, within the EACM framework, individuals can be categorized as either susceptible (S) or infected (I) in layer P , and as unaware (U) or aware (A) in layer C . This relationship is summarized as $N[t] = I[t] + S[t] = A[t] + U[t]$, where $N[t]$ signifies the total population at time t .

An additional intriguing facet of the EACM is the temporal discrepancy between its two constituent layers. Within layer P , the progression of epidemic transmission, governed by physical node contacts, unfolds at a more gradual pace compared to the dissemination of awareness within layer C . This temporal difference can be quantified by a parameter, τ . For instance, $\tau = 3$ signifies that at the moment infected nodes in layer P establish contact with their one-hop/immediate neighbors, aware nodes within layer C have already succeeded in diffusing awareness to their three-hop neighbors, concurrently. It is this precise temporal delay that imbues the study of EACM with heightened significance and complexity.

Appendix B.2 Active-Passive Immunity

In the context of epidemic propagation within the layer P , individuals in susceptible states become aware of risk information via communications in the layer C , prompting to adopt preemptive preventive measures. This process is characterized as the active immunity. Li et al. [22] quantified the neighbor contact rate of a risk-informed individual as $e^{-\mu}$, where μ symbolizes the protection degree and follows a Poisson distribution. This immunological response is encapsulated by a generalized quantitative relationship between β^A and β^U , the infection rates for aware and unaware nodes, respectively. Various studies suggested a linear correlation: $\beta^A = \gamma \cdot \beta^U$ with γ ranging between 0 and 1 [4, 9, 23, 24]. Nie et al. [25] proposed an alternative formulation: $\beta^A = k^{-\alpha} \cdot \beta^U$, $\alpha \geq 0$. Lima et al. [26] and Massaro et al. [27] defined $\beta_i^A = \beta_i^U \cdot \exp(-J \cdot s/k_i)$, where s is the number of infected neighbors. These models generally agree that $\beta^A \leq \beta^U$, but neglect the geopolitical context of nodes, such as correlation between the intensity of preventive measures and the local infection rate. For instance, a node may not immediately react if the local infection rate is 0, but is likely to adopt active measures, like self-isolation, when this rate exceeds 90%. In the light of these considerations, we propose an adaptive model for β_i^A :

$$\beta_i^A = \beta_i^U \cdot \exp\left(-\lambda \frac{\sum_{v \in \Gamma_i} I(v) + 1}{|\Gamma_i|}\right) \quad (\text{B1})$$

where $\lambda \geq 0$ is the adjustment factor, Γ_i is the community v_i belongs to, $I(v)$ is the indicative function:

$$I(v) = \begin{cases} 1, & \text{if } v \text{ is infected,} \\ 0, & \text{otherwise.} \end{cases} \quad (\text{B2})$$

Eq. (B1) acknowledges that the likelihood of adopting preventive measures varies with the proportion of infected individuals in a community.

Conversely, passive immunity refers to the immunological phenomenon where individuals' responses are primarily shaped by external influences. Def. 1 delineates a classical form of passive immunity, characterized by nodes being directed by their community's collective consciousness.

Definition 1 (Community Consciousness). Community consciousness exerts a pervasive influence across the community, embodying a consensus universally acknowledged by its members or a type of directive consistently disseminated by the most authoritative institutions or governmental bodies within that community. For example, varying awareness levels and policies across different regions lead to disparate preventive behaviors among their inhabitants.

It is noted that immunity campaigns are contingent not only upon the process of awareness propagation (i.e., active immunity) but also the mechanism of community broadcasting (i.e., passive immunity). Consequently, Eq. (B1) can be further improved as:

$$\beta_i^A = \beta_i^U \cdot k_i^{-c_i} \cdot \exp\left(-\lambda \frac{\sum_{v \in \Gamma_i} I(v) + 1}{|\Gamma_i|}\right) \quad (\text{B3})$$

where k_i denotes v_i 's in-degree, meaning that earlier protections should be arranged if v_i is popular in community. Eq. (B3) is adaptively changed according to the active and passive effects, when $c_i = 0$, β_i^U is degraded by only active immunity; when $\lambda = 0$, β_i^U is degraded by only passive immunity.

Appendix B.3 Derivation of β_c^U via MMCA

In the EACM framework, the integration of node states from both online and offline layers results in comprehensive states: Unaware and Susceptible (US), Aware and Susceptible (AS), and Aware and Infected (AI). Notably, the state of Unaware and Infected (UI) is absent as infection inherently triggers self-awareness about the epidemic. Fig. B1(a) delineates the macroscopic transition rules among these three states. Nodes in AS state transition to AI with a contagious rate β^A .

However, it is noted that the infection of a susceptible node is governed not solely by the contagion rate, but also by the node's interactions with its neighbors. For a more precise exploration, we employ a First Discrete Transition Probability Trees (FDTP) method from a microscopic perspective. Within the active-passive immunity paradigm, the FDTP can be divided into four phases: individual awareness spread (phase 1), community broadcasting (phase 2), epidemic contagion (phase 3), and self-awareness (phase 4). Each phase is meticulously incorporated into the transition trees, as depicted in Fig. B1(b).

Then, it becomes feasible to reconstitute the equations of the Microscopic Markov Chain Approach (MMCA), which articulates the probability of a node occupying a specific state at time $t + 1$ as the function of its state at the preceding time point t :

$$p_i^{\text{US}}(t + 1) = p_i^{\text{AI}}(t)\delta(1 - c_i)\mu + p_i^{\text{US}}(t)r_i(t)(1 - c_i)q_i^{\text{U}}(t) + p_i^{\text{AS}}(t)\delta(1 - c_i)q_i^{\text{U}}(t) \quad (\text{B4})$$

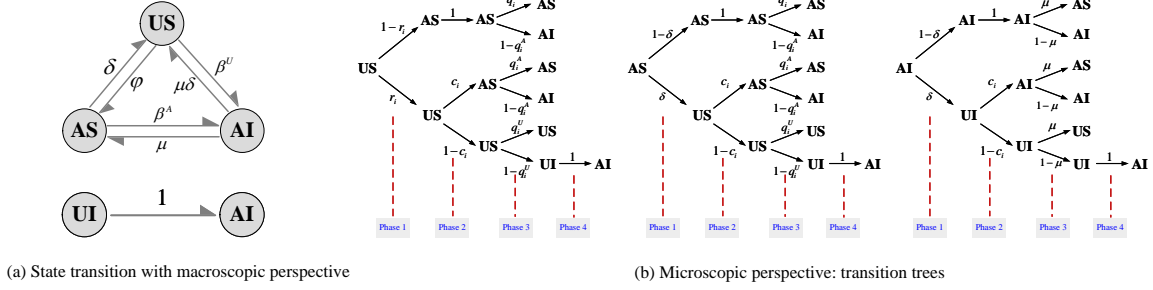


Figure B1 Macroscopic and Microscopic perspective of state transitions.

$$p_i^{\text{AS}}(t+1) = p_i^{\text{AI}}(t)[\delta c_i \mu + (1-\delta)\mu] + p_i^{\text{US}}(t) \left[r_i(t)c_i q_i^{\text{A}}(t) + (1-r_i(t))q_i^{\text{A}}(t) \right] + p_i^{\text{AS}}(t) \left[\delta c_i q_i^{\text{A}}(t) + (1-\delta)q_i^{\text{A}}(t) \right] \quad (\text{B5})$$

$$p_i^{\text{AI}}(t+1) = p_i^{\text{AI}}(t)[\delta c_i(1-\mu) + \delta(1-c_i)(1-\mu) + (1-\delta)(1-\mu)] + p_i^{\text{US}}(t)[r_i(t)c_i(1-q_i^{\text{A}}(t)) + r_i(t)(1-c_i)(1-q_i^{\text{U}}(t)) + (1-r_i(t))(1-q_i^{\text{A}}(t))] + p_i^{\text{AS}}(t)[\delta c_i(1-q_i^{\text{A}}(t)) + \delta(1-c_i)(1-q_i^{\text{U}}(t)) + (1-\delta)(1-q_i^{\text{A}}(t))] \quad (\text{B6})$$

where $p_i^{\text{US}}(t+1)$ denotes the probability of node v_i being in the US state at time $t+1$, contingent upon its own states and transition parameters at time t . c_i denotes the intensity of community broadcasting, δ and μ are recovery rates for nodes in aware and infected states, respectively. Additionally, $r_i(t)$ represents the probability that node v_i remains unactivated by its aware neighbors at time t , reflecting the influence of neighboring nodes on the state transition of v_i , $q_i^{\text{A}}(t)$ ($q_i^{\text{U}}(t)$) denotes the probability of node v_i being in aware (unaware) state, and not be infected by infectious neighbors at time t :

$$r_i(t) = \prod_j (1 - a_{ji} p_j^{\text{A}}(t) \varphi) \quad (\text{B7})$$

$$q_i^{\text{A}}(t) = \prod_j (1 - b_{ji} p_j^{\text{I}}(t) \beta_i^{\text{A}}(t)) \quad (\text{B8})$$

$$q_i^{\text{U}}(t) = \prod_j (1 - b_{ji} p_j^{\text{I}}(t) \beta_i^{\text{U}}(t)) \quad (\text{B9})$$

In accordance with the established framework, it is demonstrated that the sum of equations (B4), (B5), and (B6) is equal to 1, which facilitates the tracking of the temporal evolution of awareness and epidemic dynamics under any set of initial conditions. Moreover, a notable aspect of this model is the ability to analytically resolve the stationary state of the entire system, and enables the determination of the epidemic onset as a function of the various parameters within the model.

I. In the vicinity of the stationary state, where $t \rightarrow \infty$, it holds that $p_i(t+1) = p_i(t)$. Originating from Eq. (B6), and acknowledging the equivalence $p_i^{\text{AI}}(t) = p_i^{\text{I}}(t)$, one can deduce the following calculation:

$$p_i^{\text{I}} = p_i^{\text{I}}(1-\mu) + p_i^{\text{US}} \left[1 - q_i^{\text{A}} + r_i(1-c_i) \left(q_i^{\text{A}} - q_i^{\text{U}} \right) \right] + p_i^{\text{AS}} \left[1 - q_i^{\text{A}} + \delta(1-c_i) \left(q_i^{\text{A}} - q_i^{\text{U}} \right) \right] \quad (\text{B10})$$

II. In proximity to the onset of an epidemic, the proportion of infected individuals approaches to 0, then p_i^{I} can be approximated as $p_i^{\text{I}} = \xi_i \ll 1$, by substituting this approximation into eqs. (B8) and (B9):

$$q_i^{\text{A}} \approx \prod_j (1 - b_{ji} \xi_j \beta_i^{\text{A}}) \approx 1 - \gamma_i \beta^{\text{U}} \sum_j b_{ji} \xi_j = 1 - \gamma_i \sigma_i \quad (\text{B11})$$

$$q_i^{\text{U}} \approx \prod_j (1 - b_{ji} \xi_j \beta_i^{\text{U}}) \approx 1 - \beta^{\text{U}} \sum_j b_{ji} \xi_j = 1 - \sigma_i \quad (\text{B12})$$

in which the $o(\xi_i^2)$ terms are removed, and parameters $\gamma_i = k_i^{-c_i} \exp\left(-\lambda \frac{\sum_{v \in \mathcal{N}_i} I(v)}{|n_i|}\right)$, $\sigma_i = \beta^{\text{U}} \sum_j b_{ji} \xi_j$.

The integration of these two conditions elucidates a critical juncture indicating the onset of an epidemic under a stationary state. Consequently, it is possible to derive the phase transition point for the epidemic, characterizing the threshold at which the epidemic emerges in the system.

Firstly, substitute Eq. (B11-B12) into (B10), one can get:

$$\xi_i = (1-\mu)\xi_i + [1 - (1-c_i)(p_i^{\text{US}} r_i + p_i^{\text{AS}} \delta)] \gamma_i \sigma_i + [(1-c_i)(p_i^{\text{US}} r_i + p_i^{\text{AS}} \delta)] \sigma_i \quad (\text{B13})$$

since $\xi_i = p_i^{\text{UI}} + p_i^{\text{AI}} \ll 1$, i.e., $p_i^{\text{UI}} \approx p_i^{\text{AI}} = o(\xi_i)$, one can get $p_i^{\text{U}} = p_i^{\text{US}} + p_i^{\text{UI}} \approx p_i^{\text{US}}$, $p_i^{\text{A}} = p_i^{\text{AS}} + p_i^{\text{AI}} \approx p_i^{\text{AS}}$, and Eq. (B4) and (B5) become to:

$$p_i^{\text{U}} = p_i^{\text{U}} r_i (1-c_i) + p_i^{\text{A}} \delta (1-c_i) = (1-c_i)(p_i^{\text{U}} r_i + p_i^{\text{A}} \delta) \quad (\text{B14})$$

$$p_i^{\text{A}} = p_i^{\text{U}} (r_i c_i + 1 - r_i) + p_i^{\text{A}} (\delta c_i + 1 - \delta) \quad (\text{B15})$$

It further refines the condition that $p_i^U + p_i^A = 1$. Then, substitute Eq. (B14) into (B13), one can get:

$$0 = -\xi_i \mu + (1 - p_i^U) \gamma_i \sigma_i + p_i^U \sigma_i = -\xi_i \mu + (p_i^A \gamma_i + p_i^U) \beta^U \sum_j b_{ji} \xi_j \quad (\text{B16})$$

since $\xi_i = \sum_j E_{ij} \xi_j$, where

$$E_{ij} = \begin{cases} 1, & i = j \\ 0, & i \neq j \end{cases} \quad (\text{B17})$$

Eq. (B16) becomes to:

$$\sum_j [(p_i^A \gamma_i + p_i^U) b_{ji} - \frac{\mu}{\beta^U} E_{ij}] \xi_j = 0 \quad (\text{B18})$$

Define

$$h_{ij} = (p_i^A \gamma_i + p_i^U) b_{ji} \quad (\text{B19})$$

as the element of matrix H, then the Eq. (B18) is solvable if and only if μ/β^U is the eigenvalue of H, i.e., $\Lambda(H) = \mu/\beta^U$.

Hence, the threshold of β^U is:

$$\beta_c^U = \frac{\mu}{\Lambda_{\max}(H)} \quad (\text{B20})$$

Additionally, solve Eq. (B14) by the truth $p_i^A + p_i^U = 1$, one can get that:

$$p_i^U = \frac{\delta - \delta c_i}{1 + r_i c_i + \delta - r_i - \delta c_i} \quad (\text{B21})$$

$$p_i^A = \frac{1 + r_i c_i - r_i}{1 + r_i c_i + \delta - r_i - \delta c_i} \quad (\text{B22})$$

Upon substituting equations (B21-B22) into (B19), one can construct matrix H and consequently solve for the critical threshold β_c^U . It is noted that β_c^U is contingent upon parameters including $\varphi, \delta, c_i, \gamma_i, \mu, r_i$, and structural configurations of both the upper layer $C = \{a_{ij}\}_{n \times n}$ and lower layer $P = \{b_{ij}\}_{n \times n}$.

Appendix C Methodologies in ERSM

While direct evidence of a coupling relationship between epidemics and rumors is currently lacking, it is undeniable that the emergence of an epidemic often catalyzes the spread of rumors. The reason can be attributed to: i) psychological comfort under disease anxiety; ii) imbalance in information supply and demand under an unstable environment; iii) deliberate attack and convenient online social platform; iv) the inherent allure of rumors [28].

The ERSM concentrates on concurrently mitigate the spread of epidemics and rumors. The present study frames this challenge as a Multi-Objective Optimization (MOO) problem, focusing on the development of containment strategies that not only reducing the prevalence of infection and rumors, but also ensuring cost-effectiveness. Compared to addressing them separately, the MOO model offers two principal benefits:

- i) Flexible budgeting: Traditional methods struggle to predict the effectiveness of specific cost expenditures in achieving containment. While our model mitigates this issue by offering a spectrum of scenarios across varying costs.
- ii) Multiple strategies: This method can provides a range of containment strategies, facilitating a comprehensive overview and more informed decisions on effectively managing both epidemics and rumors.

Appendix C.1 The Multi-Objective Optimization Model

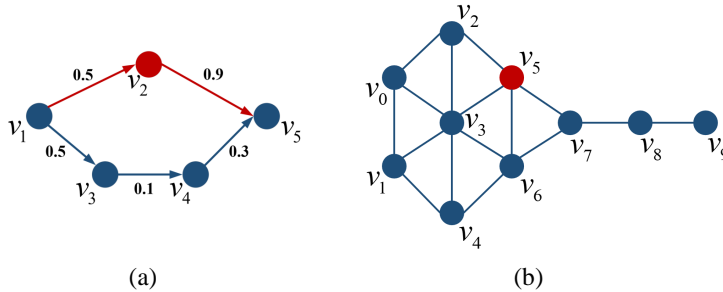


Figure C1 Instances for (a) β PWC calculation; (b) MOO problem solving, it sets $\beta = 0.1, p^T = p^R = 1, \Delta_c = 0.005$.

Appendix C.1.1 Minimizing the Connectivity of Epidemic Network

Timely supervision often faces challenges due to factors like the incubation period of the disease and the presence of asymptomatic carriers, which can impede the effectiveness of containment strategies. An increasing body of research advocates for early vaccination as a more efficient, cost-effective, and globally applicable immunization strategy. Building upon this insight, we propose a novel objective: the removal (i.e., vaccination) of a specific set of nodes that minimizes the connectivity of the entire network.

The PairWise Connectivity (PWC), a prevalent metric in CNP problem is adopted to measure the connectivity of the epidemic network after vaccinating a set of nodes.

$$npwc(G') = \frac{1}{n(n-1)} \sum_{v_i, v_j \in V, v_i \neq v_j} p(v_i, v_j) \quad (C1)$$

where G' is the graph after removing vaccinated nodes and their corresponding edges. The connectivity $p(v_i, v_j)$ is 1 if the node pair (v_i, v_j) is connected via a path in G' . Clearly, it holds that $npwc(G') \in [0, 1]$, and a lower $npwc$ value indicates a more effective removal(vaccination) effect.

However, due to the stronger connectivity of the social network, the removal of nodes will not necessarily lead to the disintegration of the network, rendering $npwc$ less applicable in the epidemic containment problem. On the other hand, the infection rate β also worth consideration, for instance, even if a node v has high centrality within the network topology, if $\beta_v = 0$, vaccinating this node will not yield any significant protective effects for its neighbors. Such β -based protective utility is termed as the β PU. When nodes pair (v_i, v_j) remains connected via a path, the probability of v_i infecting v_j is determined by aggregating the probabilities across all possible paths from v_i to v_j ,

$$\Delta_{ij} = \sum_{l \in L} \prod_{(s,t) \in l} \beta_{st} \quad (C2)$$

Then, an improved metric incorporating β PU into Eq. (C1) is shown as:

$$\beta pwc(G') = \frac{1}{n(n-1)} \sum_{v_i, v_j \in V, v_i \neq v_j} p'(v_i, v_j) \quad (C3)$$

where

$$p'(v_i, v_j) = \begin{cases} 1, & \text{if } \Delta_{ij} \geq \Delta_c, \\ 0, & \text{otherwise.} \end{cases} \quad (C4)$$

Δ_c is a predefined threshold, when Δ_{ij} exceeds Δ_c , it is considered that v_i has a significant potential impact on v_j . As illustrated in Fig. C1(a), when setting $\Delta_c = 0.1$, $\Delta_{15} = 0.5 * 0.9 + 0.5 * 0.1 * 0.3 = 0.465 > 0.1$, then $p'(v_1, v_5) = 1$. While after vaccinating node v_2 , $\Delta_{15} = 0.5 * 0.1 * 0.3 = 0.015 < 0.1$, consequently, $p'(v_1, v_5) = 0$. It suggests that vaccinating v_2 can effectively reduce the connection, hence decreasing value of $npwc$.

The metric βpwc effectively integrates the β PU, accounting for the likelihood of infection transmission along the network paths, thereby enhancing the metric relevance and applicability in the context of epidemic control. In this refined framework, a lower value of βpwc indicates a more effective disruption or collapse of the epidemic network, signifying a successful containment strategy.

Therefore, the primary objective function revolves around identifying an optimal subset of nodes, $S, S \subseteq V$, so that the removal (vaccination) of S can minimize the βpwc :

$$\begin{aligned} & \text{Minimize } F_1(S) \\ & \text{where } F_1(S) = \beta pwc(V \setminus S), S \subseteq V \end{aligned} \quad (C5)$$

Appendix C.1.2 Minimizing the Rumor Propagation

A practical approach to suppress rumor is to introduce the truthful information, thereby setting up a competitive dynamic in the network. Once individuals receive truth, they not only stop accepting rumors but also begin disseminating the truth to others [18]. This process can be modeled as a Competitive Independent Cascade (CIC) model, with truth acting as a countermeasure to rumor proliferation.

Competitive independent cascade (CIC): Both rumor and truth spread through the network following the Independent cascade (IC) model. Once a node is activated by the truth, it becomes immune to rumor, and vice versa. Importantly, if a node is exposed to both rumor and truth simultaneously, it will preferentially adopt the truth. The CIC model can be defined as a 3-tuple $(G(V, E), p^R, p^T)$ where G represents a directed graph, p^R and p^T are activation probabilities of rumors and truths, respectively. To differentiate the impact of truth from rumors, we set $p^T = \alpha \cdot p^R$, where $\alpha \in (0, 1/p^R]$ is an adjustment factor. The influence diffusion function is denoted as $\sigma_R(S^T)$, evaluating the expected number of final rumor-adopted nodes under the initial rumor-active seeds R and truth-active seeds S^T .

Therefore, the second objective function is focused on identifying an optimal set of nodes $S^T, S^T \subseteq V \setminus R$, so that the activation of S^T for propagation of truth can minimize the $\sigma_R(S^T)$:

$$\begin{aligned} & \text{Minimize } F_2(S) \\ & \text{where } F_2(S) = \sigma_R(S), S \subseteq V \setminus R \end{aligned} \quad (C6)$$

Appendix C.1.3 Minimizing the Associated Costs

The third objective function addresses the cost aspect of containment measures for both the epidemic and the spread of rumors. These containment strategies, while effective, incur certain inevitable costs, making cost minimization an essential component of the MOOP framework. The costs can be categorized as: i) vaccination costs $c_1(\cdot)$, which is set as a constant value, e.g., $c_1(v) = 0.5$ for all $v \in V$; ii) truth-Deployment costs $c_2(\cdot)$, which is set as $c_2(v) = \frac{k_v}{n-1}$, $v \in V$, where k_v denotes degree of v , under the premise that more influential nodes (such as opinion leaders) typically require higher incentives or efforts to disseminate information. Then, the third objective function of minimizing the total costs can be mathematically represented as follows:

$$\begin{aligned} & \text{Minimize } F_3(S) \\ & \text{where } F_3(S) = c_1(S) + c_2(S) \end{aligned} \quad (C7)$$

In summary, the entire multi-objective optimization function is to integrate three objective functions:

$$\begin{aligned} & \text{Minimize } F(S) = (F_1(S), F_2(S), F_3(S))^T \\ & \text{where } F_1(S) = \beta pwc(V \setminus S), \\ & \quad F_2(S) = \sigma_R(S), \\ & \quad F_3(S) = c_1(S) + c_2(S) \end{aligned} \quad (C8)$$

Appendix C.2 The NSGAI-D Algorithm

Encoding and decoding process: A candidate solution S to Eq. (C8) is encoded as an integer string of length $|V|$, with each element adopting values from $\{0, 1, 2, 3\}$. Here, “0” indicates no action is taken on the corresponding network node. Values “1”, “2”, and “3” indicate the node is targeted for vaccination, truth activation, or both of the above, respectively. Conversely, Decoding S involves mapping these integers to specific nodes. For example, for $S = \{0, 0, 1, 0, 1, 2, 3, 0\}$, which can be decoded as $S_1 = \{0, 0, 1, 0, 1, 0, 1, 0\} = \{v_2, v_4, v_6\}$ for $F_1(S_1)$, $S_2 = \{0, 0, 0, 0, 0, 1, 1, 0\} = \{v_5, v_6\}$ for $F_2(S_2)$, and $S_3 = S_1 \cup S_2 = \{v_2, v_4, v_5, v_6\}$ for $F_3(S_3)$, effectively mapping the strategy for each objective.

Algorithm C1 Init_pop(\cdot)

Require: Multiplex network $G(V, E_1, E_2)$, z, q .

Ensure: Initial populations with size zq .

```

1: initial pop,  $j \leftarrow 0$ 
2: # step 1: ensuring diversity;
3:  $F_3^{min}, F_3^{max} \leftarrow F_3(\emptyset), F_3(V)$ 
4:  $\tilde{F}_3 \leftarrow \{F_3^{min} + i \cdot (F_3^{max} - F_3^{min})/z | i = 0, 1, \dots, z\}$ 
5: # step 2: ensuring accelerating convergence;
6: Vac_cdd: rank nodes of  $G(V, E_1)$  in descending order according to closeness/betweenness centrality;
7: Tru_cdd: rank nodes of  $G(V, E_2)$  in descending order according to degree centrality;
8: while  $F_3'$  in  $\tilde{F}_3$  do
9:   while  $j < q/2$  do
10:      $w \leftarrow \text{random}()$ 
11:     select  $S_1$  from Vac_cdd with constraint  $c_1(S_1) = w \cdot F_3'$ , and  $S_2$  from Tru_cdd with constraint  $c_2(S_2) = (1 - w) \cdot F_3'$ ;
12:     sample  $S'_1, S'_2$  from  $V$  randomly, where  $|S'_1| = |S_1|$  and  $|S'_2| = |S_2|$ .
13:     encode  $(S_1, S_2)$  as  $pop^i$ ,  $(S'_1, S'_2)$  as  $pop^{i+1}$ 
14:      $pop \leftarrow pop \cup \{pop^i, pop^{i+1}\}$ 
15:      $j \leftarrow j + 1$ 
16:   end while
17: end while
18: return pop.
```

Fig. C1(b) illustrates an example of computing Eq. (C8), v_5 colored in red is the initial rumor-active individual. For two solutions $S_A = \{0, 0, 0, 3, 0, 0, 0, 0, 0\}$ and $S_B = \{0, 0, 0, 1, 0, 0, 2, 0, 0\}$, one can calculate that $F_1(S_A) = F_1(S_B) \approx 0.583$, $F_2(S_A) = |\{v_5, v_7, v_8, v_9\}| = 4$, $F_2(S_B) = |\{v_2, v_5\}| = 2$, $F_3(S_A) = 0.5 + 6/9 \approx 1.167$, $F_3(S_B) = 0.5 + 4/9 \approx 0.944$. Hence, $S_B \succ S_A$.

The trade-off between containment effects (F_1 and F_2) and associated costs (F_3) presents a complex optimization challenge. While a simplistic strategy might involve allocating separate budgets to distinct targeted algorithms, this approach may overlook more efficient solutions. In contrast, the NSGAI-D algorithm, leveraging the Pareto front, offers a comprehensive array of solutions that balance these competing objectives effectively. To evaluate the Pareto optimal frontier under varying budgetary and cost constraints, and to ensure a diverse solution set, we propose a centrality-based method for initial population generation in Alg. C1.

For $F_3(\cdot)$, its bounds are established as $F_3^{max} = F_3(\{3, 3, \dots, 3\}) = 0.5 \cdot n + \bar{k}$ for the upper limit, and $F_3^{min} = F_3(\{0, 0, \dots, 0\}) = 0$ for the lower limit, where \bar{k} is the average degree. To ensure solution diversity, the algorithm employs equidistant selection for F_3 , as detailed in lines 3-4, with a uniform distribution of z values drawn from the interval $[F_3^{min}, F_3^{max}]$. Then, to facilitate rapid convergence, lines 6-7 utilize centrality rankings to inform the initial population generation. In the subsequent steps (lines 8-17), for each $F_3', F_3' \in \tilde{F}_3$, a random weight $w, w \in (0, 1)$ is dedicated to derive two node sets S_1 and S_2 , constrained by $c_1(S_1) = w \cdot F_3'$ and $c_2(S_2) = (1 - w) \cdot F_3'$, respectively, where $c_1(\cdot), c_2(\cdot)$ are as defined in Eq. (C7). Simultaneously, corresponding sets S'_1 and S'_2 of equal size to S_1 and S_2 are randomly generated. This process results in an initial generation of zq populations, laying the groundwork for the optimization procedure.

Algorithm C2 NSGAI-D

Require: Multiplex network $G(V, E_1, E_2)$, $z, q, max.t$.

Ensure: Pareto optimal solution.

```

1:  $t, N \leftarrow 0, z \cdot q$ 
2:  $P_t \leftarrow \text{Init\_pop}(G, z, q)$ 
3: while  $t < max.t$  do
4:    $Q_t \leftarrow \text{genetic}(P_t)$ 
5:    $R_t \leftarrow P_t \cup Q_t$ 
6:    $\Gamma \leftarrow \text{fast\_non\_dominated\_sort}(R_t)$ 
7:    $P_{t+1}, i \leftarrow \emptyset, 1$ 
8:   while  $|P_{t+1}| + |\Gamma_i| \leq N$  do
9:      $P_{t+1} \leftarrow P_{t+1} \cup \Gamma_i$ 
10:     $i \leftarrow i + 1$ 
11:   end while
12:   crowding\_distance\_assignment( $\Gamma_i$ )
13:    $P_{t+1} \leftarrow P_{t+1} \cup \Gamma_i[1 : (N - |P_{t+1}|)]$ 
14:    $t \leftarrow t + 1$ 
15: end while
16: return  $\Gamma_1$ .
```

Alg. C2 delineates the modified NSGAI-D framework, specifically tailored for addressing the discrete multi-objective optimization problem as formulated in Eq. (C8). Within this framework, the *genetic*(\cdot) function encompasses the suite of genetic

operators, namely selection, crossover, and mutation, which are instrumental in generating the offspring population. The practical implementation of these genetic operations is visually represented in Fig. C2. Additionally, *fast_non_dominated_sort*(\cdot) and *crowding_distance_assignment*(\cdot) are two classical operators of NSGA-II algorithm, with the former sorting the population based on non-dominance levels, and the latter assigning a crowding distance to each solution.

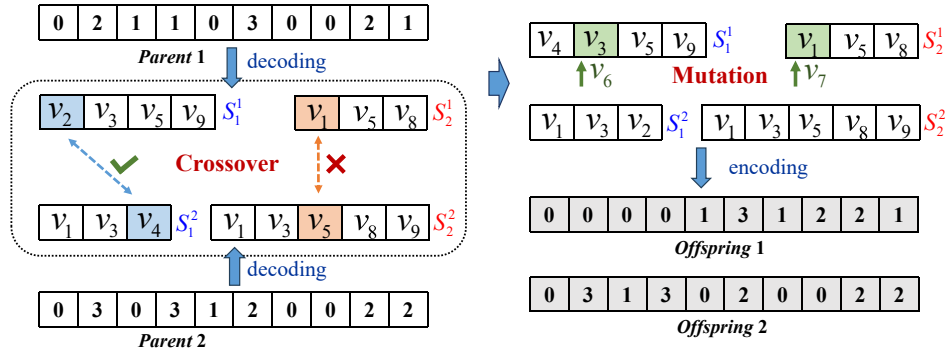


Figure C2 Genetic process example.

Appendix D Experiments

Appendix D.1 Experimental Settings

Given the absence of real-world datasets that fully capture the characteristics of the EACM, the present paper combines various single-layer networks. For the epidemic spreading layer $P := \langle V, E_P \rangle$, community-based topologies like LFR or SBM networks are suitable as they mimic offline physical contact patterns. Conversely, for the information spreading layer $C := \langle V, E_C \rangle$, there are two main construction strategies: i) enhancing connectivity by adding new links to E_P , or ii) generating synthetic networks that mirror the scales of V , and epitomize characteristics typical of online social networks. The composition and attributes of the datasets employed in this approximation approach are detailed in Tab. D1.

Table D1 Attributes of datasets.

| | P | Generation of C | # V | # Ep | # Ec | Ave_deg of {P, C} | # Comms |
|-------------|-------------|------------------------|--------|---------|---------|-------------------|---------|
| Multiplex 1 | LFR1 | add edges | 8,000 | 26,130 | 78,339 | { 6.53, 19.58} | 207 |
| Multiplex 2 | LFR2 | incorporate with WS | 12,000 | 54,000 | 120,000 | { 9.10, 20.00} | 136 |
| Multiplex 3 | LFR3 | incorporate with BA | 15,000 | 224,775 | 224,775 | {29.27, 29.27} | 60 |
| Multiplex 4 | WS | add edges | 6,000 | 60,000 | 179,541 | {20.00, 59.85} | 36 |
| Multiplex 5 | SBM | incorporate with Email | 1,005 | 7,562 | 24,929 | {15.05, 49.61} | 30 |
| Multiplex 6 | Karate Club | add edges | 34 | 78 | 215 | { 4.59, 12.67} | 2 |

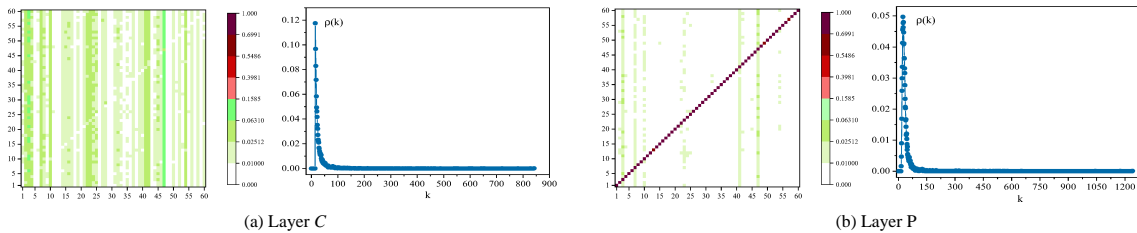


Figure D1 Community-based density matrices and Degree distribution histograms of two layers of Multiplex 3.

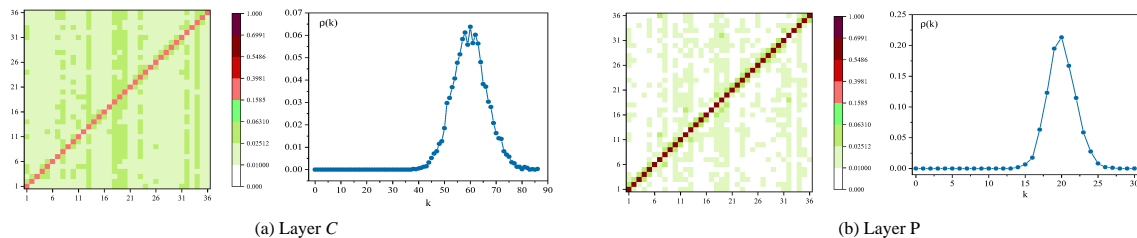


Figure D2 Community-based density matrices and Degree distribution histograms of two layers of Multiplex 4.

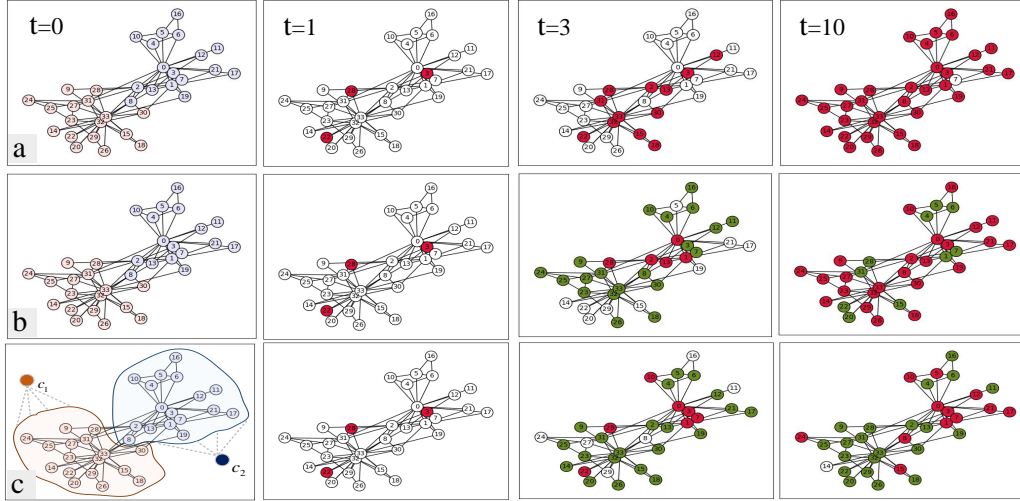


Figure D3 Snapshots of nodes states evolution on Karate graph, where US, AS, AI are colored in white, green and red, respectively. Snapshots of (a) epidemic evolution; (b) active immunity-based epidemic evolution; (c) active-passive immunity-based epidemic evolution. It sets $\varphi = 0.2$, $\delta = 0.1$, $\beta^U = 0.3$, $\mu = 0.2$, $\lambda = 1$, $\tau = 2$, $c_1 = 0.8$ and $c_2 = 0.2$.

To effectively showcase the properties of the datasets, a community-based density matrix is constructed. Suppose network P encompasses q communities: $\{c_1, c_2, \dots, c_q\}$, then define matrix $\mathcal{C} = \{c_{ij}\}_{q \times q}$, where

$$c_{ij} = \frac{\#links(c_i \rightarrow c_j)}{\sum_{k=1}^q \#links(c_i \rightarrow c_k)} \quad (\text{D1})$$

$\#links(c_i \rightarrow c_j)$ counts the number of links from c_i to c_j . Fig. D1 and D2 display the community density matrices and degree histograms of Multiplex 3 and Multiplex 4, respectively. We can find that both layers of Multiplex 3 conform to a power-law degree distribution. Notably, in layer P , intra-community links are markedly denser compared to inter-community links, indicating a strong community-based structure. Conversely, in layer C , the distribution of links exhibits a lesser degree of influence from the community structure, suggesting a more dispersed and less clustered network topology.

Appendix D.2 Numerical Simulations

Appendix D.2.1 Part A: Experiments and Results in EACM

Fig. D3 delineates the evolutionary process of epidemics under different conditions. Initially infecting three nodes, the figures demonstrate varied outcomes at $t = 10$: in (a), where only epidemic spreads, 97% of nodes are infected; in (b), where epidemic is coupled with the active awareness, infection proportion drops to 71%; and in (c), where epidemic is incorporated with both active and passive effects, the infection proportion further declines to 35%. These trends highlight the effectiveness of active-passive actions in mitigating epidemic spread. Notably, stronger community influence, as indicated by $c_1 = 0.8$ versus $c_2 = 0.2$, demonstrates greater efficacy in controlling the epidemic.

Fig. D4 - D9 systematically verify the impacts of six parameters: c_i , λ , μ , φ , δ , and τ , on the epidemic spread. In each panel, the heatmap graph correlates the fraction of infected nodes (FIN) at the terminal time with β^U and the respective parameter under consideration. The color gradation in these heatmaps, demarcated at 0, 1%, 5%, 10%, etc., illustrating varying levels of epidemic spread, with the assumption that a 1% FIN signifies the critical threshold for the onset of an epidemic. Additionally, the Star-dotted line in each panel represents the solutions of β_c^U calculated by Eq. (B20). These graphical representations provide a visual validation of the MMCA's predictions against the simulated outcomes, elucidating the influence of each parameter on the dynamics of epidemic spread.

For each node v_i , the passive impact originating from its communities (c_i) is defined in two distinct manners: i) c_i is drawn from a uniform distribution ranging from $Rc - 0.1$ to Rc ; ii) $c_i = Sc/|\Gamma_i|$, where Rc and Sc are scale factors, $|\Gamma_i|$ denotes the size of the community to which v_i belongs. In Fig. D4, an inverse relationship is observed between the magnitude of c_i (either Rc or Sc) and the proportion of infected nodes in both multiplex 1 and 2. Specifically, when $\beta^U = 0.1$, a high community passive impact (with $Rc = 0.7$) effectively controls the epidemic. Moreover, the results obtained from the MMCA align well with the phase transitions observed in the heatmap pattern, demonstrating the accuracy and applicability of the MMCA in predicting epidemic dynamics under varying levels of community passive impact.

The parameter λ functions analogously to c_i , but specifically pertains to the influence of active awareness within a community. As depicted in Fig. D5, an increase in λ corresponds to heightened sensitivity of nodes to epidemic awareness within their community, leading to more stringent protective behaviors. Notably, when the value of λ is greater than or equal to 10, the epidemic can effectively be controlled at a β^U value of 0.05. This trend underscores the significant role of active awareness in mitigating epidemic spread, where higher λ values reflect a community's enhanced responsiveness to the epidemic threat and consequent adoption of preventive measures.

The parameter μ is pivotal in influencing both the evolution of the epidemic and the calculation of its threshold. Fig. D6(a) illustrates the qualitative impact of increasing μ on the FIN. Notably, when $\mu = 0.5$, the FIN remains below 50% even when β^U reaches 1. This observation is particularly encouraging the significant contribution of μ . However, it is difficult to improve μ by manual intervention, for an efficient epidemic containment strategy, the other parameters within the EACM, such as c_i and λ , may synergistically contribute to the overall effectiveness of strategies.

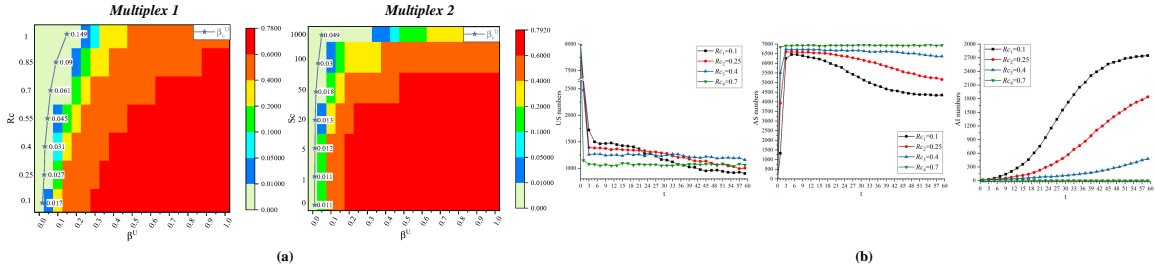


Figure D4 (a) Fraction of infected nodes in terms of c_i and β^U on Multiplex 1 and 2; (b) numbers of node states (US, AS, AI) in evolutionary process Multiplex 1. It sets $\lambda = 1$, $\mu = 0.2$, $\varphi = 0.1$, $\delta = 0.1$, $\tau = 2$ for (a), $\beta^U = 0.1$ for (b).

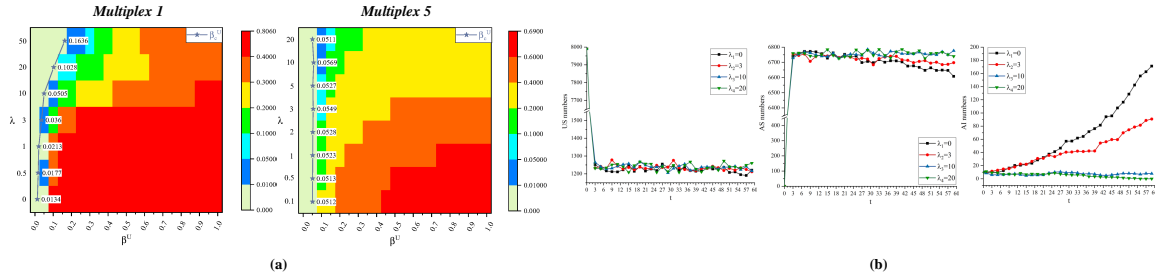


Figure D5 (a) Fraction of infected nodes in terms of λ and β^U on Multiplex 1 and 5; (b) numbers of node states (US, AS, AI) in evolutionary process of Multiplex 1. It sets $Rc = 0.3$, $\mu = 0.2$, $\varphi = 0.2$, $\delta = 0.1$, $\tau = 2$ for (a), $\beta^U = 0.05$ for (b).

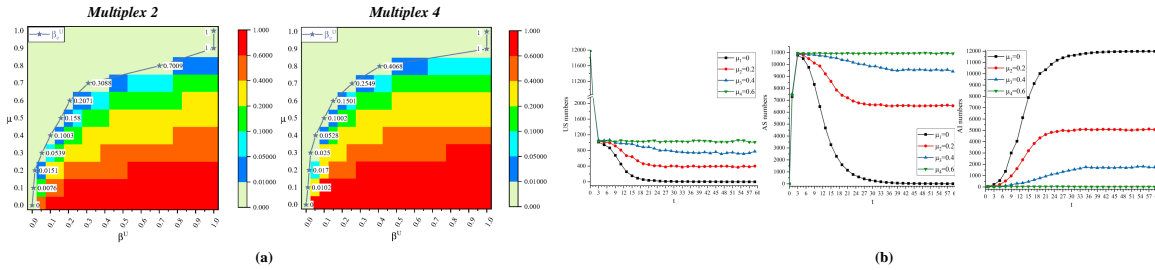


Figure D6 (a) Fraction of infected nodes in terms of μ and β^U on Multiplex 2 and 4; (b) numbers of node states (US, AS, AI) in evolutionary process of Multiplex 2. It sets $Rc = 0.3$, $\lambda = 2$, $\varphi = 0.1$, $\delta = 0.05$, $\tau = 2$ for (a), $\beta^U = 0.2$ for (b).

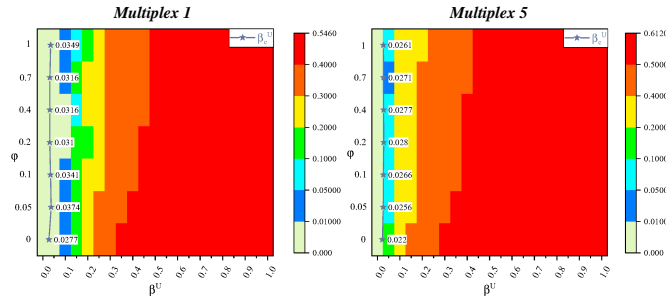


Figure D7 Fraction of infected nodes in terms of φ and β^U on Multiplex 1 and 5. It sets $Rc = 0.3$, $\mu = 0.3$, $\lambda = 3$, $\delta = 0.1$, $\tau = 2$.

Fig. D7-D9 delve into the impacts of the parameters φ , δ and τ on EACM. A key observation from these figures is that variations in these parameters have a minimal impact on the FIN across most values of β^U . Although φ , δ and τ play roles in the evolution of the UAU-SIS model and contribute to the calculation of the epidemic threshold β_c^U , both simulation and numerical results suggest that their influence on β_c^U is relatively minor. However, it is worth recognizing that, despite their limited effect on the epidemic threshold, these parameters can still significantly influence the FIN at non-threshold points. This influence is often modulated by network's topology and other parameters. Thus, while their direct impact on the threshold may be small, φ , δ and τ are still integral to a comprehensive understanding of epidemic dynamics.

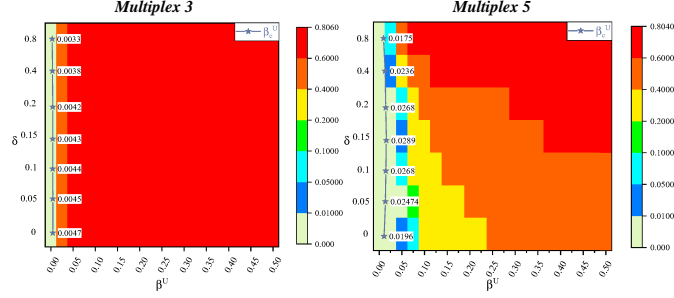


Figure D8 Fraction of infected nodes in terms of δ and β^U on Multiplex 3 and 5. It sets $R_c = 0.3$, $\mu = 0.2$, $\lambda = 1$, $\varphi = 0.2$, $\tau = 2$.

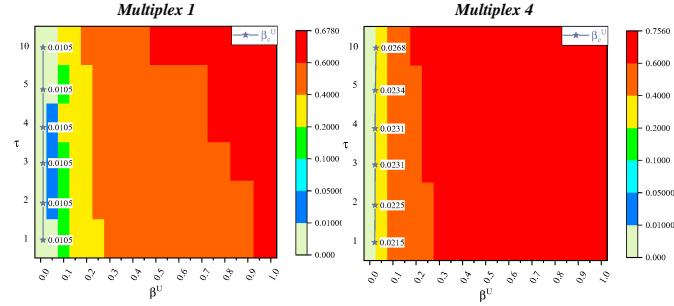


Figure D9 Fraction of infected nodes in terms of τ and β^U on Multiplex 1 and 4. It sets $R_c = 0.3$, $\mu = 0.2$, $\lambda = 3$, $\delta = 0.05$, $\varphi = 0.1$.

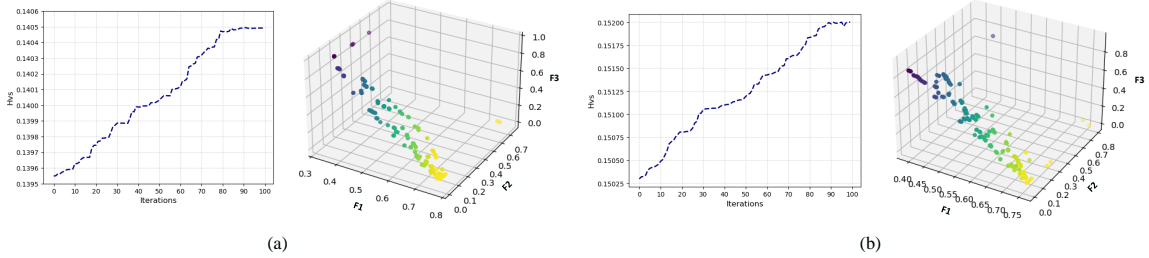


Figure D10 The Hvs and PF diagrams achieved by NSGAI-D. (a) and (b) are under parameter settings i) and ii), respectively.

Appendix D.2.2 Part B: Experiments and Results in ERSM

To assess the efficacy of the NSGAI-D algorithm, two distinct numerical experiments are performed on Multiplex 5 with two different sets of parameter configurations, respectively.

- i) $z = 30$, $q = 6$, $p_c = 0.01$, $p_m = 0.005$, $\Delta_c = 0.0005$, $\beta = 0.1$, $p^R = 0.15$, $p^T = 0.18$, $max_iter = 100$;
- ii) $z = 50$, $q = 4$, $p_c = 0.05$, $p_m = 0.01$, $\Delta_c = 0.0005$, $\beta = 0.1$, $p^R = 0.2$, $p^T = 0.22$, $max_iter = 100$.

Fig. D10 depicts the iterative convergence process of the NSGAI-D algorithm by a well-established metric in evolutionary computing: the Hypervolume (HV) [29], and also provides the corresponding Pareto front at the end of iterations. An observable trend in both scenarios is the gradual improvement in the quality of the solutions as the number of iterations increases. The algorithm eventually converging towards an optimal or near-optimal set of solutions. In PF of panel (a), the algorithm initializes with 180 populations, ultimately yielding 126 Pareto optimal solutions. These solutions represent the optimal strategies for different budget levels (as defined by F_3 values). For instance, if a manager seeks to minimize both the connectivity of the epidemic network and the spread of rumors, all within a budget of no more than 0.38, (s)he can identify several Pareto optimal solutions that satisfy the condition $F_3 \leq 0.38$. One such solution, S^* , for example, achieves an F_1 value of 0.6997, and an F_2 value of 0.0121. Furthermore, by querying solution space, the specific strategy entailed in S^* involves vaccinating nodes in $S_1^* = \{v_7, v_{11}, v_{15}, \dots\}$, and activating nodes in $S_2^* = \{v_2, v_9, v_{11}, \dots\}$ to propagate truth. Additionally, in both panel (a) and (b), several PF values are situated at the extremities, such as (0.7589, 0.7414, 0), (0.7589, 0.7013, 0.1510), which also represent Pareto optimal values, since when $F_3 = 0$, indicating no budget allocation for node selection, solutions that can dominate this scenario do not exist, i.e., $S = \{0, \dots, 0\}$ is naturally belongs to the PF.

Table D2 NSGAI-D V.S Greedy under setting 1.

| pop | NSGAI-D | | | Greedy | |
|------|----------------|--------|--------|----------|--------|
| | F1 | F2 | F3 | F1_g | F2_g |
| 1 | 0.7589 | 0.7414 | 0 | 0.7589 | 0.7414 |
| 2 | 0.7542 | 0.0198 | 0.0679 | 0.7535 | 0.0179 |
| 3 | 0.7473 | 0.0152 | 0.1388 | 0.7475 | 0.015 |
| 4 | 0.7085 | 0.0172 | 0.2051 | 0.7056 | 0.0155 |
| 5 | 0.7586 | 0.0109 | 0.3161 | 0.7565 | 0.0147 |
| 6 | 0.6997 | 0.0121 | 0.3761 | 0.7036 | 0.0147 |
| 7 | 0.7298 | 0.0109 | 0.4691 | 0.7276 | 0.0144 |
| 8 | 0.5607 | 0.0143 | 0.5795 | 0.5581 | 0.0143 |
| 9 | 0.4769 | 0.0246 | 0.6534 | 0.4708 | 0.0207 |
| 10 | 0.4307 | 0.0282 | 0.7591 | - | 0.0271 |
| 11 | 0.3854 | 0.0229 | 0.8925 | - | 0.02 |
| 12 | 0.371 | 0.0153 | 0.9959 | - | 0.0131 |
| T(s) | 4825.86 | | | 41878.57 | |

Table D3 NSGAI-D V.S Greedy under setting 2.

| pop | NSGAI-D | | | Greedy | |
|------|-----------------|--------|--------|----------|--------|
| | F1 | F2 | F3 | F1_g | F2_g |
| 1 | 0.7589 | 0.7865 | 0 | 0.7589 | 0.7865 |
| 2 | 0.7545 | 0.1034 | 0.017 | 0.7492 | 0.1033 |
| 3 | 0.7139 | 0.0132 | 0.2 | 0.7105 | 0.0128 |
| 4 | 0.751 | 0.0112 | 0.3088 | 0.7492 | - |
| 5 | 0.6618 | 0.0117 | 0.3959 | 0.6572 | 0.0119 |
| 6 | 0.6881 | 0.0111 | 0.4573 | 0.6796 | - |
| 7 | 0.6566 | 0.0114 | 0.5088 | 0.6403 | 0.0111 |
| 8 | 0.6153 | 0.0113 | 0.5693 | 0.6187 | 0.0113 |
| 9 | 0.551 | 0.0116 | 0.6604 | 0.5491 | 0.0118 |
| 10 | 0.485 | 0.0202 | 0.7265 | - | 0.0303 |
| 11 | 0.4879 | 0.0127 | 0.8158 | - | 0.0123 |
| 12 | 0.4665 | 0.0109 | 0.9884 | - | - |
| T(s) | 11838.16 | | | 52635.19 | |

To verify the validity of NSGAI-D algorithm, we conduct comparative analyses against a high-performance greedy algorithm, noted for its capacity to secure a minimum $1 - 1/e$ approximation of the optimal solution when the objective function exhibits submodularity. The validation methodology encompassed the following steps: firstly, sample 12 non-dominated populations ($pop1, pop2, \dots, pop12$) evenly across the Pareto front generated by NSGAI-D, focusing on their F3 values. Subsequently, derive the associated costs, c_1 and c_2 , based on their F1 and F2 metrics, respectively. Finally, apply the greedy algorithm to determine the optimal values of two objective functions, denoted as F1.g and F2.g, under the constraints imposed by c_1 and c_2 , respectively. For example, taking $pop2$ from Tab.D2 with $F1 = 0.7542$ and $F2 = 0.0198$, one can decode $pop2$ into S_1 and S_2 , thereby deriving their constraints c_1 and c_2 . These constraints are integrated into Eqs.(C5) and (C6), respectively, and upon solving with the greedy algorithm, yield outcomes of 0.7535 for F1.g and 0.0179 for F2.g, respectively.

Tabs.D2 and D3 delineate the outcomes of comparative experiments conducted under settings i) and ii), respectively, showcasing the metrics F1, F2, and F3 in the second, third, and fourth columns. Given the greedy algorithm's intrinsic focus on single-objective optimization, modifications are made to accommodate the multi-objective framework of Eqs (C5) and (C6) using constraints c_1 and c_2 , with results tabulated in the fifth and sixth columns. Notations of "-" in both tables signal instances unassessed due to prohibitive computational requirements. For the greedy algorithm, cessation of operation is predicated on exceeding a 10-hour computational threshold.

The performance of the NSGAI-D algorithm is affirmed through dual dimensions:

1) Effectiveness analysis: Comparative scrutiny of F1 with F1.g and F2 with F2.g unveils the greedy algorithm's marginal superiority, attributed to its potent search mechanism. Nonetheless, the nominal variance between the algorithms underscores a parallel in effectiveness, reinforcing the NSGAI-D's competitive stance.

ii) Efficiency assessment: Operational efficiency is gauged by juxtaposing the algorithms' execution durations. Here, NSGAI-D conspicuously outperforms, with the greedy algorithm's runtime surpassing NSGAI-D's by factors of 8.68 and 4.45 in Tabs. D2 and D3, correspondingly. Unlike its counterpart, NSGAI-D, through a singular computational instance, furnishes a comprehensive suite of Pareto optimal solutions, heralding substantial efficiency gains. This capability furnishes decision-makers with a nuanced framework to equilibrate containment efficacy against fiscal prudence.

In essence, NSGAI-D's proficiency in generating an expansive spectrum of Pareto optimal solutions epitomizes a more integrated and flexible strategy for navigating the complexities of containment dilemmas, underscoring its value in multifaceted decision-making landscapes.

Appendix E Contributions and Future Works

This study introduces two innovative mechanisms: the EACM and ERSM, which enhance understanding of meme propagation dynamics within coupled online-offline networks. The principal contributions are as follows:

In EACM: 1) The introduction of a community-structured physical contact layer, implementing an Active-Passive Epidemic Immunity (APEI) strategy that integrates online awareness with offline community effects. Comparative analyses with other state-of-the-art literature are detailed in Tab.E1. 2) The development of a Microscopic Markov Chain Approach (MMCA) with a novel community broadcasting phase to derive the epidemic threshold. 3) Validation of numerical and simulation results across six artificially synthesized multiplex networks.

In ERSM: 4) The formulation of a Multi-Objective Optimization (MOO) problem to minimize epidemic spread, rumor propagation, and associated costs concurrently. 5) The design of an infection rate-based pairwise connectivity metric to evaluate nodes' abilities in reducing the connectivity of the epidemic network; 6) The enhancement of the NSGAI-D algorithm with centrality-based initialization to boost diversity and convergence speed.

The integrated network model, intertwining online and offline domains, presents a captivating and pragmatic framework. Future enhancements to this model are planned, with an emphasis on expanding its application to broader social communication contexts, including virtual reality (VR) and mixed reality (MR) technologies. Community-based epidemic modeling is anticipated to inform the development of a "divide and conquer" vaccination strategy, which could be incorporated into the EACM to establish a novel epidemic suppression framework that leverages the interdependencies among awareness, vaccination, and epidemic spread. There-after, the associated MMCA process is expected to incorporate a new state transition phase: Vaccination. Furthermore, delving deeper into the intricate interrelation between epidemic proliferation and rumor circulation, and developing more sophisticated metaheuristic algorithms tailored for solving discrete multi-objective optimization challenges are warrant extensive exploration in forthcoming research endeavors.

Table E1 Comparison of main studies in EACM.

| Studies | Coupling Effects on Epidemic | Immune Strategy | Quantification of Immune Behavior | Characteristics of Layers |
|--|-----------------------------------|-----------------|---|-------------------------------|
| Granell et al. [3], Gao et al. [30], and Feng et al. [9] | awareness | active | $\beta^A = \gamma\beta^U, \gamma \in [0, 1]$ | normal |
| Granell et al. [4], Ma et al. [31], and Xia et al. [32] | awareness, mass-media | active, passive | $\beta^A = \gamma\beta^U, \gamma \in [0, 1]$ | normal |
| Guo et al. [33] | awareness (local) | active | $\beta^A = 0$ | normal |
| Yang et al. [7] | awareness | active | $\beta^A = \gamma\beta^U, \gamma \in [0, 1]$ | time-varying |
| Nie et al. [25] | awareness | active | $\beta^A = k^{-\alpha}\beta^U, \alpha \geq 0$ | heterogeneous |
| Liu et al. [5] | awareness (local) | active | $\beta^A = k^{-\alpha}\beta^U, \alpha \geq 0$ | normal |
| Yin et al. [6], and Li et al. [34] | awareness, vaccination | active | $\beta^V = \gamma\beta^U, \gamma \in [0, 1]$ | three-layer |
| Wang et al. [35] | positive/negative awareness | active | $\beta^A = \gamma\beta^U, \gamma \in [0, 1]$ | normal |
| Guo et al. [8] | awareness | active | $\beta^A = \gamma\beta^U, \gamma \in [0, 1]$ | partial-mapping, time-varying |
| Our study | awareness, community-broadcasting | active, passive | $\beta_i^A = \beta_i^U \cdot k_i^{-c_i} \cdot \exp(-\lambda \frac{\sum_{v \in \Gamma_i} I(v)+1}{ \Gamma_i })$ | community-structured |

References

- Li X J, Li C, Li X. The impact of information dissemination on vaccination in multiplex networks. *Science China Information Sciences*, 2022, 65: 172202.
- Funk S, Gilad E, Watkins C, et al. The spread of awareness and its impact on epidemic outbreaks. *Proceedings of the National Academy of Sciences*, 2009, 106: 6872-6877.
- Granell C, Gómez S, Arenas A. Dynamical interplay between awareness and epidemic spreading in multiplex networks. *Physical review letters*, 2013, 111: 128701.
- Granell C, Gómez S, Arenas A. Competing spreading processes on multiplex networks: awareness and epidemics. *Physical review E*, 2014, 90: 012808.
- Liu L, Feng M, Xia C, et al. Epidemic trajectories and awareness diffusion among unequals in simplicial complexes. *Chaos, Solitons & Fractals*, 2023, 173: 113657.
- Yin Q, Wang Z, Xia C, et al. Impact of co-evolution of negative vaccine-related information, vaccination behavior and epidemic spreading in multilayer networks. *Communications in Nonlinear Science and Numerical Simulation*, 2022, 109: 106312.
- Yang H, Gu C, Tang M, et al. Suppression of epidemic spreading in time-varying multiplex networks. *Applied Mathematical Modelling*, 2019, 75: 806-818.
- Guo H, Yin Q, Xia C, et al. Impact of information diffusion on epidemic spreading in partially mapping two-layered time-varying networks. *Nonlinear Dynamics*, 2021, 105: 3819-3833.
- Feng M, Li X, Li Y, et al. The impact of nodes of information dissemination on epidemic spreading in dynamic multiplex networks. *Chaos: An Interdisciplinary Journal of Nonlinear Science*, 2023, 33.
- Xie M, Li Y, Feng M, et al. Contact-dependent infection and mobility in the metapopulation SIR model from a birth?death process perspective. *Chaos, Solitons & Fractals*, 2023, 177: 114299.
- Deb K, Pratap A, Agarwal S, et al. A fast and elitist multiobjective genetic algorithm: NSGA-II. *IEEE transactions on evolutionary computation*, 2002, 6: 182-197.
- Zitzler E, Laumanns M, Thiele L. SPEA2: Improving the strength Pareto evolutionary algorithm. *TIK report*, 2001, 103.
- Zhang Q, Li H. MOEA/D: A multiobjective evolutionary algorithm based on decomposition. *IEEE Transactions on evolutionary computation*, 2007, 11: 712-731.
- Del Ser J, Osaba E, Molina D, et al. Bio-inspired computation: Where we stand and what's next. *Swarm and Evolutionary Computation*, 2019, 48: 220-250.
- Faramondi L, Setola R, Panzieri S, et al. Finding critical elements in infrastructure networks. *International Journal of Critical Infrastructure Protection*, 2017.
- Faramondi L, Oliva G, Panzieri S, et al. Network structural vulnerability: a multiobjective attacker perspective. *IEEE Transactions on Systems, Man, and Cybernetics: Systems*, 2018, 49: 2036-2049.
- Zhang L, Xia J, Cheng F, et al. Multi-objective optimization of critical node detection based on cascade model in complex networks. *IEEE Transactions on Network Science and Engineering*, 2020, 7: 2052-2066.
- Gong Y, Liu S, Bai Y. Influence Minimization With Conformity-Aware Competitions. *IEEE Systems Journal*, 2023, 17: 3706-3717.
- Biswas T K, Abbasi A, Chakraborty R K. An improved clustering based multi-objective evolutionary algorithm for influence maximization under variable-length solutions. *Knowledge-Based Systems*, 2022, 256: 109856.
- Sheikhahmadi A, Zareie A. Identifying influential spreaders using multi-objective artificial bee colony optimization. *Applied Soft Computing*, 2020, 94: 106436.

- 21 Gomez S, Diaz-Guilera A, Gomez-Gardenes J, et al. Diffusion dynamics on multiplex networks. *Physical review letters*, 2013, 110: 028701.
- 22 Li Y, Zeng Z, Feng M, et al. Protection degree and migration in the stochastic SIRS model: A queueing system perspective. *IEEE Transactions on Circuits and Systems I: Regular Papers*, 2021, 69: 771-783.
- 23 Zhu L, Liu W, Zhang Z. Interplay between epidemic and information spreading on multiplex networks. *Mathematics and Computers in Simulation*, 2021, 188: 268-279.
- 24 Kan J Q, Zhang H F. Effects of awareness diffusion and self-initiated awareness behavior on epidemic spreading-an approach based on multiplex networks. *Communications in Nonlinear Science and Numerical Simulation*, 2017, 44: 193-203.
- 25 Nie X, Tang M, Zou Y, et al. The impact of heterogeneous response on coupled spreading dynamics in multiplex networks. *Physica A: Statistical Mechanics and its Applications*, 2017, 484: 225-232.
- 26 Lima A, De Domenico M, Pejovic V, et al. Exploiting cellular data for disease containment and information campaigns strategies in country-wide epidemics. *arXiv preprint arXiv:1306.4534*, 2013.
- 27 Massaro E, Bagnoli F. Epidemic spreading and risk perception in multiplex networks: A self-organized percolation method. *Physical Review E*, 2014, 90: 052817.
- 28 Tasnim S, Hossain M M, Mazumder H. Impact of rumors and misinformation on COVID-19 in social media. *Journal of preventive medicine and public health*, 2020, 53: 171-174.
- 29 Bader J, Zitzler E. HypE: An algorithm for fast hypervolume-based many-objective optimization. *Evolutionary computation*, 2011, 19: 45-76.
- 30 Gao B, Deng Z, Zhao D. Competing spreading processes and immunization in multiplex networks. *Chaos, Solitons & Fractals*, 2016, 93: 175-181.
- 31 Ma W, Zhang P, Zhao X, et al. The coupled dynamics of information dissemination and SEIR-based epidemic spreading in multiplex networks. *Physica A: Statistical Mechanics and its Applications*, 2022, 588: 126558.
- 32 Xia C, Wang Z, Zheng C, et al. A new coupled disease-awareness spreading model with mass media on multiplex networks. *Information Sciences*, 2019, 471: 185-200.
- 33 Guo Q, Jiang X, Lei Y, et al. Two-stage effects of awareness cascade on epidemic spreading in multiplex networks. *Physical Review E*, 2015, 91: 012822.
- 34 Li L, Dong G, Zhu H, et al. Impact of multiple doses of vaccination on epidemiological spread in multiple networks. *Applied Mathematics and Computation*, 2024, 472: 128617.
- 35 Wang Z, Xia C, Chen Z, et al. Epidemic propagation with positive and negative preventive information in multiplex networks. *IEEE transactions on cybernetics*, 2020, 51: 1454-1462.